Rapid Communications

$\mathcal{L}^2$ localization landscape for highly excited states

Loïc Herviou and Jens H. Bardarson
Department of Physics, KTH Royal Institute of Technology, SE-106 91 Stockholm, Sweden

(Received 17 April 2020; accepted 2 June 2020; published 11 June 2020)

The localization landscape [M. Filoche and S. Mayboroda, Proc. Natl. Acad. Sci. USA **109**, 14761 (2012)] gives direct access to the localization of bottom-of-band eigenstates in noninteracting disordered systems. We generalize this approach to eigenstates at arbitrary energies in systems with or without internal degrees of freedom by introducing a modified $\mathcal{L}^2$ landscape, and we demonstrate its accuracy in a variety of archetypal models of Anderson localization in one and two dimensions. This $\mathcal{L}^2$-landscape function can be efficiently computed using hierarchical methods that allow evaluating the diagonal of a well-chosen Green's function. We compare our approach to other landscape methods, bringing insights on their strengths and limitations. Our approach is general and can in principle be applied to both studies of topological Anderson transitions and many-body localization.

DOI: 10.1103/PhysRevB.101.220201

Introduction. The theoretical discussion of Anderson localization, the strict confinement of matter waves to a finite subspace due to destructive quantum interference, dates back to 1958 [1]. Progress since then has come in bursts, often separated by long intervals. Only after over 20 years did mathematical proofs start to appear [2,3] and the scaling theory of localization was introduced [4], suggesting that all eigenstates in low dimensions are localized. Two major recent modern developments involve the interplay of localization with topology and interactions: Surfaces of topological insulators [5] resist localization [6–8] and extended bulk states are obtained at the transition between two topologically distinct insulating phases [9–14]. Interactions give rise to many-body localization, in which an eigenstate phase transition is obtained at energies high above the ground state [15–19]. These phenomena only started to be understood in the last couple of decades.

One reason for this slow progress may be that localization is due to nontrivial interference patterns that are not easily guessed from the random potential the particles move in. There is generally no obvious correlation between the localization centers of wave functions and the potential extrema. In a sense, this means that there is no obvious classical starting point from which one can do simple perturbation theory. Now, in a series of fascinating work, such a starting point may have been identified in the so-called localization landscape [20–28]. The localization landscape can be seen as the inverse of an effective potential obtained from the initial random potential, and it has the property that its peaks and valleys predict the location of the few lowest-energy localized wave functions. It furthermore gives the correct integrated density of states [29] at low energy from a simple Weyl law, which otherwise badly fails when using the original potential.

The original formulation [20] of the localization landscape is for scalar field theories with a real and positive Green's function, and applies strictly only to low-energy states close to the bottom of the energy spectrum. These constraints prevent direct applications to many of the modern approaches mentioned above, where the interesting physics often takes place in states at or near the middle of the spectrum. Here, we introduce an extension of the localization landscape, which we coin the $\mathcal{L}^2$ landscape, that faithfully captures the localization of eigenstates at all energies and in the presence of internal degrees of freedom. The $\mathcal{L}^2$ landscape can be *efficiently* numerically obtained in generic physical models, in the absence of long-range hopping. We exemplify its validity and reliability through several archetypal models of localization in one and two dimensions. This landscape is applicable to both topological models and many-body Hamiltonians and can therefore be used to analyze most localization problems.

An alternative extension of the localization landscape to Dirac fermions was recently introduced by Lemut *et al.* in Ref. [30]. This method, based on the comparison matrix [31,32], has the advantage that is retains the simplicity of the original landscape, and can be applied to Dirac Hamiltonians with inner degrees of freedom. Neither the original landscape nor the one based on the comparison matrix can, however, describe a generic high-energy state as does our $\mathcal{L}^2$ landscape, albeit at the cost of a slightly reduced efficiency. We conclude our work by briefly comparing our method to these alternatives, bringing insights into the strengths and weaknesses of conventional localization landscape approaches.

$\mathcal{L}^2$ localization landscape. In their original paper [20], Filoche and Mayboroda considered the localization of a scalar field, or equivalently of spinless fermions. Let H be the corresponding single-particle Hamiltonian and $|\phi^\beta\rangle$ an eigenstate of H with eigenvalue E^β. We denote by $\phi^\beta_j = \langle j|\phi^\beta\rangle$

its amplitude at site j. By application of the inverse of the Hamiltonian, one straightforwardly obtains

$$|\phi_j^\beta| = \left| E^\beta \sum_m (H^{-1})_{j,m} \phi_m^\beta \right| \tag{1}$$

$$\leqslant |E^\beta| \|\phi^\beta\|_\infty \sum_m |(H^{-1})_{j,m}| \equiv |E^\beta| \|\phi^\beta\|_\infty u_j. \tag{2}$$

u is called the localization landscape. The key insight of Ref. [20] was to realize that in a wide class of models, H^{-1} can have all components positive, implying that u is a solution to the differential equation

$$Hu = 1. \tag{3}$$

The requirement of elementwise positivity of H^{-1} enforces strong restriction on H: It must be a monotone matrix [33], a class of matrices that is generally hard to characterize. In the case of a real symmetric matrix with all off-diagonal (hopping) terms negative, such as in the standard Anderson model, a necessary and sufficient condition is that H is positive definite. The localization landscape proves to tightly bound bottom-of-band eigenstates, almost saturating Eq. (2), in a wide variety of models [20]. This saturation implies that the lowest-energy eigenstates are localized at the peaks of the landscape and different eigenstates are separated by landscape minima. Indeed, we can rewrite the localization landscape as

$$u_j = \sum_\beta \frac{\phi_j^\beta}{E^\beta} \sum_m \phi_m^\beta. \tag{4}$$

By construction, due to the inverse energy factor, eigenstates with the lowest energy will contribute more to the localization landscape than ones at higher energies. On the other hand, high-energy states are not accurately localized by the landscape. This landscape can therefore not be used to study center-of-band properties.

We propose to overcome this limitation by slightly modifying the definition of the localization landscape. Starting from Eq. (1), we apply the Cauchy-Schwartz inequality to obtain

$$|\phi_j^\beta| \leqslant |E^\beta| \|\phi^\beta\|_2 \sqrt{\sum_n (H^{-1})_{j,n} (H^{-1})^*_{j,n}} \tag{5}$$

$$= |E^\beta| \sqrt{(\mathcal{M}^{-1})_{j,j}}, \tag{6}$$

where $\mathcal{M} = H^\dagger H$ is a Hermitian positive-definite matrix and we assume normalized eigenfunctions with $||\phi^\beta||_2 = 1$. The $\mathcal{L}^2$-landscape $u^{(2)}$ is then defined by

$$u_j^{(2)} = \sqrt{(\mathcal{M}^{-1})_{j,j}}. \tag{7}$$

$\mathcal{M}$ is invertible as long as H is invertible, and the inequalities are valid whether H is Hermitian or non-Hermitian. The largest contributions to the landscape $u^{(2)}$ are from the eigenstates with the smallest absolute energy. With this definition, there is no requirement that H be positive definite, and we can therefore explore localization at all energies by simply shifting the Hamiltonian by a constant real factor E_T. Note also that the normalization by the largest element of ϕ^β has vanished, replaced by its 2-norm (equal to 1 by convention). The change in normalization can conveniently help to differentiate localized and delocalized regimes. In the original formulation, several tightly localized but close-in-energy eigenstates would have exactly the same landscape signatures as a state delocalized on a subpart of the system (with well-separated peaks) as the difference in amplitude of the wave functions is not taken into account. Equation (7) is valid in the continuum limit, and can be straightforwardly applied to systems with internal degrees of freedom.

To ensure that $\mathcal{M}$ can be inverted, it is convenient to introduce a complex energy shift ε and work with the matrix $\tilde{H} = H + i\varepsilon\,\mathrm{Id}$. The energy in the bound is then renormalized to $E_\varepsilon^\beta = |E^\beta + i\varepsilon| = \sqrt{(E^\beta)^2 + \varepsilon^2}$. ε should be smaller than the level spacing at the probed energy in order to resolve the different eigenstates. In the presence of modes exactly at the target energy, for example, due to symmetries, it can nonetheless be interesting not to choose an arbitrarily low cutoff, so that the zero modes do not completely dominate the landscape. The level spacing itself can be readily estimated from any approximation W of the bandwidth and the Hamiltonian dimension N as W/N and a typical safe choice for ε would be $W/(10N)$. We can gain an intuition for this by writing, for an Hermitian Hamiltonian, the square of the landscape as

$$\left(u_j^{(2)}\right)^2 = \sum_\beta \frac{\left|\phi_j^\beta\right|^2}{(E^\beta - E_T)^2 + \varepsilon^2}, \tag{8}$$

where we have now also explicitly included the real energy shift E_T. We therefore have that

$$\varepsilon \left(u_j^{(2)}\right)^2 \underset{\varepsilon \to 0}{\longrightarrow} \rho_j(E_T), \tag{9}$$

where $\rho_j(E) = \sum_\beta |\phi_j^\beta|^2 \delta(E - E^\beta)$ is the local density of states at site j and energy E. This explains why the $\mathcal{L}^2$ landscape provides an efficient description of states close to E_T, while the presence of the factor of ε on the left-hand side of relation (9) means that states further away from E_T also contribute to the landscape.

The $\mathcal{L}^2$ localization landscape can be computed efficiently, even if it does not satisfy a simple (discrete) differential equation. Indeed, for short-ranged Hamiltonians, numerous methods have been developed to compute the diagonal of the Green's functions efficiently, such as hierarchical algorithms [34–38] (that can also take advantage of the positive definiteness of $\mathcal{M}$). More refined algorithms in two dimensions [39–41] can compute the diagonal of the inverse in $O(L^3)$ operations, where L is the linear dimension of the two-dimensional system. Moreover, several methods [42–44] exist to numerically derive upper bounds on the components of the inverse of Hermitian definite positive matrices, that can readily be applied here.

Anderson model. We first illustrate our method in the prototypical one-dimensional Anderson model for localization, with Hamiltonian

$$H = -t \sum_j (c_j^\dagger c_{j+1} + c_{j+1}^\dagger c_j) + \sum_j V_j c_j^\dagger c_j. \tag{10}$$

c_j ($c_j^\dagger$) is the fermionic annihilation (creation) operator on site j, t is the hopping amplitude (set to 1 in the following), and V_j is a random on-site potential uniformly distributed in

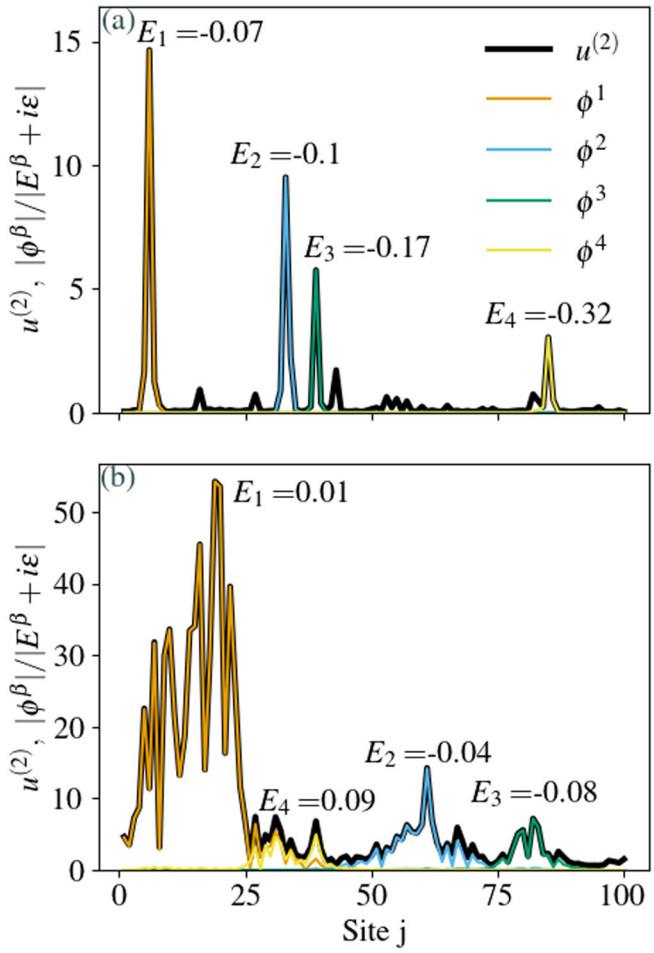

FIG. 1. $\mathcal{L}^2$ landscape and the four eigenstates closest to zero energy ($E_T = 0$) in the Anderson model for disorder strengths (a) $W = 25$ and (b) $W = 2$. The eigenstates are normalized by their energy and $\varepsilon = 10^{-3}$ is fixed to be smaller than the typical mean level spacing. The different peaks in the localization landscape coincide with the different eigenstates and their location. The low minima form domain bounds that separate different eigenstates at low energy. $u^{(2)}$ predicts accurately the localization and ordering of the states in all cases, and tightly bounds the localization of these states.

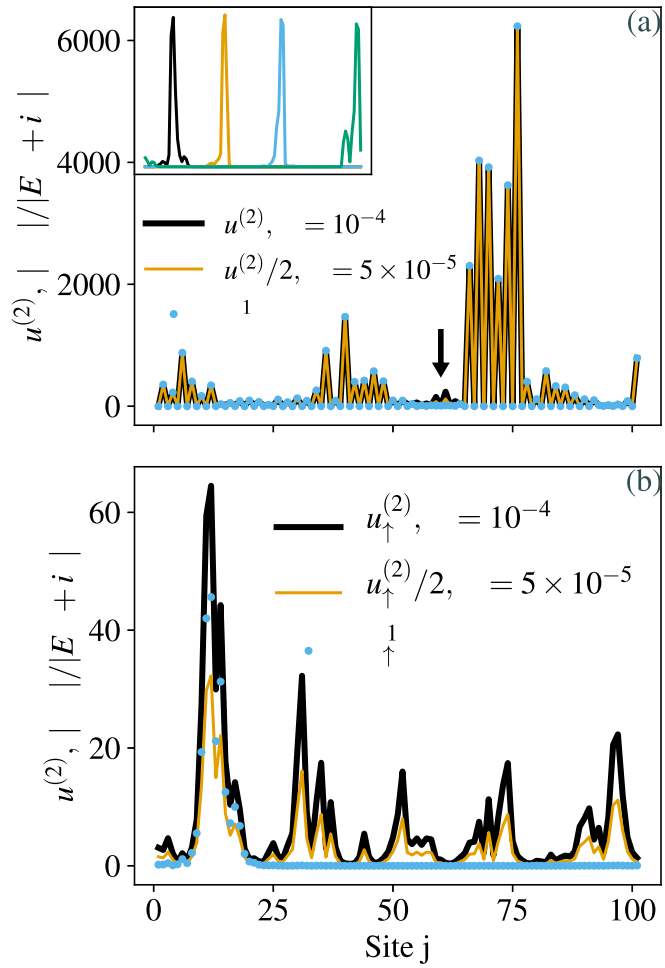

FIG. 2. The $\mathcal{L}^2$ localization landscape at $E_T = 0$ for two values of ε and the lowest lying eigenstate in the (a) one-channel and (b) two-channel chiral Anderson model, for $V_0 = 4$ and $L = 101$ sites. We only plot the spin-up component of the landscapes and wave functions in the two-channel case for simplicity; the other component can be obtained by symmetry. For one channel, there exists an extended zero mode which gives a clear contribution to the landscape, with an amplitude that scales as ε^{-1}. Conversely, the part of the landscape that does not scale with ε (shown by the arrow) corresponds to higher-energy states. In the inset we show, for reference, the wave functions of the four states in the bulk of the band with $E_T = V_0$. For two channels, there is no zero mode, and the lowest-energy states are localized. The rescaled landscape does not match its initial counterpart. The landscape is a less tight bound than usual due to the chiral symmetry which doubles the number of states. To get a tighter bound one can split the pairs of states at $\pm E$ by a weak breaking of the symmetry.

$[-W, W]$. An arbitrarily weak disorder is enough to localize all eigenstates at all energies in the thermodynamic limit, including in the middle of the spectrum. In Fig. 1 we show the $\mathcal{L}^2$ localization landscape at zero energy in a chain of $L = 100$ sites with open boundary conditions, and compare it with the few eigenstates nearest in energy. Taking the cutoff ε to be smaller than the typical level spacing, $u^{(2)}$ accurately describes the localization of the states close to $E_T = 0$ at both strong and weak disorder. As with the conventional landscape, many eigenstates are captured by a single computation of the landscape, whether at strong or weak disorder. The ordering of peak amplitudes matches the eigenstate ordering.

Chiral Anderson model. The ability to access arbitrary energies allows us to access more refined properties of localization, such as due to the presence of symmetries. In one dimension, the presence of chiral symmetry leads to an even-odd effect in terms of the number of channels [7,45]; indeed, due to the symmetry, states either come in pairs $(E, -E)$ or have zero energy. For an odd number of channels (and an odd number of sites at finite sizes) there therefore must exist a symmetry protected zero-energy eigenstate. This zero-energy state is delocalized even in the presence of strong disorder. In Fig. 2(a), we compare the $\mathcal{L}^2$ localization landscape and eigenstates of the minimal single-channel chiral Hamiltonian

$$H = -\sum_j t_j c_j^\dagger c_{j+1} + \text{H.c.}, \tag{11}$$

with t_j taken uniformly in $[-V_0, V_0]$.

Though the landscape may appear similar to the one obtained in Fig. 1, we can identify that most peaks are contributions of a zero mode by varying the cutoff ε. Indeed, the energy in Eq. (6) is given by $|E^\beta + i\varepsilon|$. When $\varepsilon \to 0$, the contributions to the landscape of states with nonzero energy are suppressed compared to the divergent contribution of the zero-energy eigenstates and we can identify the zero-mode contributions by computing the landscape for two different cutoffs: Bounds of the zero modes will scale as the inverse of ε. Note that due to the zero mode, choosing a very low value of ε leads to a better description of the delocalized mode, while a value closer to the level spacing gives more information on the localization of the neighboring states. In Fig. 2(a), we show an example with such a delocalized state. Additionally, around $j = 60$, one can see a few peaks where the landscape does not scale linearly with ε; this is where the first excited states are localized. In the absence of degeneracies, it is then immediate to identify that the zero mode spans a large part of the system. One can verify by shifting the energy reference E_T that bulk states are localized.

Conversely, in the case of an even number of channels, the symmetry no longer guarantees the presence of a zero mode, and the eigenstates close to zero energy are all localized. The Hamiltonian

$$H = -t \sum_j \vec{c}_j{}^\dagger \sigma^z \vec{c}_{j+1} + \text{H.c.} - \sum_j V_j \vec{c}_j{}^\dagger \sigma^y \vec{c}_{j+1} + \text{H.c.}, \tag{12}$$

with $\vec{c} = (c_\uparrow, c_\downarrow)$ two fermionic species, σ^α with $\alpha = x, y, z$ the Pauli matrices and $V_j \in [-V_0, V_0]$, is an example of two-channel chiral Anderson model. The chiral symmetry is realized by

$$\sigma^x H \sigma^x = -H. \tag{13}$$

As shown in Fig. 2(b), there are no zero modes and the eigenstate closest to zero energy is now localized. The localization landscape bounds the eigenstates less tightly than in the previous examples due to the chiral symmetry: States come in pairs of opposite energies which have exactly the same renormalized energies and a similar local polarization. These two contributions therefore sum up constructively and strongly relax the usual tightness of the bound. This can be remediated by a small breaking of the chiral symmetry with a nonzero E_T smaller than the mean level spacing.

Dirac fermions in two dimensions. Finally, we demonstrate that the $\mathcal{L}^2$ landscape also captures the (absence of) localization of Dirac fermions in two dimensions. Single Dirac cones with time reversal are not localized at any energy [7,46–48], and belong to different universality classes depending on the form of the disorder. A convenient lattice model to simulate a single Dirac cone is a critical two-dimensional Chern insulator on a square lattice,

$$H = -t \sum_{\langle \vec{r}, \vec{r}' \rangle} \left(\vec{c}_{\vec{r}}{}^\dagger \sigma^z \vec{c}_{\vec{r}'} + \text{H.c.} \right) - \mu \sum_{\vec{r}} \vec{c}_{\vec{r}}{}^\dagger \sigma^z \vec{c}_{\vec{r}} \tag{14}$$

$$+ \Delta_x \sum_{\vec{r}} (i \vec{c}_{\vec{r}}{}^\dagger \sigma^x \vec{c}_{\vec{r}+\vec{e}_x} + \text{H.c.}) \tag{15}$$

$$+ \Delta_y \sum_{\vec{r}} (i \vec{c}_{\vec{r}}{}^\dagger \sigma^y \vec{c}_{\vec{r}+\vec{e}_y} + \text{H.c.}). \tag{16}$$

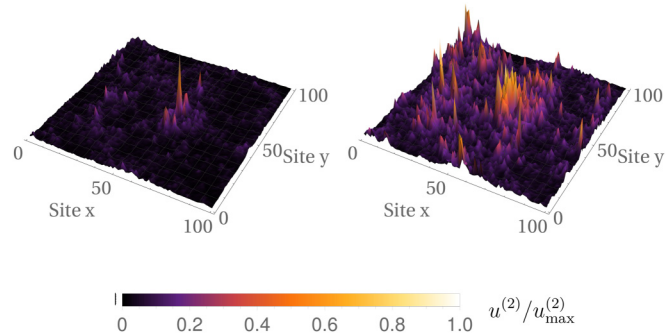

FIG. 3. $\mathcal{L}^2$ localization landscape for the critical two-dimensional Chern insulator in the presence of all types of disorder for both spin components (left: spin up; right: spin down). We fix $V_0^\alpha = 2t$, $\varepsilon = 10^{-5}$, and study states at $E_T = 0$. In both graphs, the vertical component depicts the low-level eigenstates, while the color scale is the corresponding normalized value of the landscape. Peaks and valleys in the landscape match the lowest-energy eigenstates.

t, Δ_x, and Δ_y act as different flavors of spin-orbit coupling, and μ is a chemical potential. The system falls into class D with the particle-hole symmetry

$$\sigma^x H^* \sigma^x = -H. \tag{17}$$

For $\mu = \pm 4t$ and Δ_x and Δ_y nonzero, the Hamiltonian is at a critical point between a topological phase with Chern number ± 1 and a trivial phase. It presents a single Dirac cone at momentum $\vec{k} = (0, 0)$ for $\mu = -4t$ and $\vec{k} = (\pi, \pi)$ for $\mu = 4t$. We place ourselves at this phase transition and introduce all possible random local perturbations,

$$V^a = \sum_{\vec{r}, a} V^a_{\vec{r}} \vec{c}_{\vec{r}}{}^\dagger \sigma^a \vec{c}_{\vec{r}}, \tag{18}$$

with $a \in \{0, x, y, z\}$ and $V^a_{\vec{r}}$ taken uniformly in $[-V_0^a, V_0^a]$. V^0 is a random scalar potential, V^z a random mass, and $V^{x/y}$ random chiral hoppings. The random mass V^z preserves the particle-hole symmetry, while the other potential terms break the symmetry such that the system falls directly into class A. In class D, at weak disorder, the system would fall into the thermal quantum Hall transition fixed point, before transitioning at higher disorder to a metallic phase, as long as the disorder averages to zero [7,49–52]. In class A on the other hand, the model flows towards the integer quantum Hall transition fixed point, though with strong finite-size effects that will lead to apparent localization at strong disorder and higher-energies [7,48,53–55]. In Fig. 3, we compare the prediction of the localization landscape for the critical Chern insulator and the actual low-energy eigenstates in the presence of all types of disorder, for the two spin components. Similar results are obtained in the D class. Peaks and valleys in the landscape match the ones in the eigenstates, both exactly at zero energy where the gap closes, but also deep in the band. We do observe the absence of localization close to zero energy, as is evident by looking at the spin-down component.

Discussion. We have introduced the $\mathcal{L}^2$ landscape, an extension of the localization landscape that can be used to

characterize eigenstates of a Hamiltonian in the bulk spectrum of arbitrary models. This requires the computation of the diagonal of the inverse of the positive-definite matrix $\mathcal{M} = H^\dagger H$. It provides an accurate and tight bound, in the absence of degeneracies, on the localization or delocalization of eigenstates at an arbitrary energy. We have demonstrated the power of this landscape in a variety of models in one and two dimensions, with and without internal degrees of freedom, and presenting mobility edges and other nontrivial localization properties. In all these examples, our method successfully and accurately pinpointed the eigenstates closest to any target energy.

It is pertinent to compare our results to other landscape-based approaches. In particular, the comparison-matrix landscape introduced in Ref. [30] can in principle be used to study states in the middle of the spectrum. In practice, the comparison matrix needs to be positive definite, which, in the models we considered, requires the introduction of the same shift ε we introduced. Instead of being a small control parameter, however, this shift is much larger than the mean level spacing and sometimes even of the order of the bandwidth. The energy denominator in Eq. (4) (replacing the Hamiltonian by the comparison matrix) is then strongly flattened, with all eigenstates contributing with similar amplitudes. The obtained landscape is then no longer a good predictor of the localization of the eigenstates closest to the target energies (see the Supplemental Material [56] for more details). These are generic limitations in conventional landscape methods, as long as the energy gap to the lowest eigenstate is much larger than the level spacing. This problem can be alleviated by certain types of disorder that make the Hamiltonian diagonal dominant, and therefore allow for small ε, such as discrete disorder distributions or disorder of the form $V\vec{n}\cdot\vec{\sigma}$, with V a large constant amplitude and $\vec{n}$ a random unit vector, representing strongly disordered magnetic impurities.

The generality of our approach—including both interacting systems (in configuration space, for example), non-Hermitian models and continuous models—is straightforward as it only requires the invertibility of the Hamiltonian, that can be shifted by a small $\varepsilon \in \mathbb{C}$. In particular, the possibility of targeting accurately highly excited states may prove useful for applications to many-body localization [57], though the high coordination number of the equivalent Anderson lattice may limit a purely numerical computation. For possible future directions, we note that wave functions at the Anderson transition point are known to exhibit multifractal behavior [53,58–64]. The properties of the critical point can be identified by computing the fractal dimension of the wave function. How to generalize these ideas to the localization landscape, as the latter does not describe a single eigenstate, but a superposition of several with weight depending on their energies, is an interesting open question.

We thank Carlo Beenakker, Vardan Kaladzhyan, Edwin Langmann, and Björn Sbierski for useful discussions. This work was supported by the ERC Starting Grant No. 679722, the Roland Gustafsson's Foundation for Theoretical Physics, and the Karl Engvers foundation.

[1] P. W. Anderson, Absence of diffusion in certain random lattices, Phys. Rev. **109**, 1492 (1958).
[2] I. Goldshtein, S. Molchanov, and L. Pastur, Pure point spectrum of stochastic one dimensional Schrödinger operators, Funct. Anal. Appl. **11**, 1 (1977).
[3] H. Kunz and B. Souillard, Sur le spectre des opérateurs aux différences finies aléatoires, Commun. Math. Phys. **78**, 201 (1980).
[4] E. Abrahams, P. W. Anderson, D. C. Licciardello, and T. V. Ramakrishnan, Scaling Theory of Localization: Absence of Quantum Diffusion in Two Dimensions, Phys. Rev. Lett. **42**, 673 (1979).
[5] M. Z. Hasan and C. L. Kane, Colloquium: Topological insulators, Rev. Mod. Phys. **82**, 3045 (2010).
[6] A. P. Schnyder, S. Ryu, A. Furusaki, and A. W. W. Ludwig, Classification of topological insulators and superconductors in three spatial dimensions, Phys. Rev. B **78**, 195125 (2008).
[7] F. Evers and A. D. Mirlin, Anderson transitions, Rev. Mod. Phys. **80**, 1355 (2008).
[8] A. W. W. Ludwig, Topological phases: classification of topological insulators and superconductors of non-interacting fermions, and beyond, Phys. Scr. **2016**, 014001 (2015).
[9] P. W. Brouwer, C. Mudry, B. D. Simons, and A. Altland, Delocalization in Coupled One-Dimensional Chains, Phys. Rev. Lett. **81**, 862 (1998).
[10] T. Senthil, M. P. A. Fisher, L. Balents, and C. Nayak, Quasiparticle Transport and Localization in High-T_c Superconductors, Phys. Rev. Lett. **81**, 4704 (1998).
[11] I. A. Gruzberg, A. W. W. Ludwig, and N. Read, Exact Exponents for the Spin Quantum Hall Transition, Phys. Rev. Lett. **82**, 4524 (1999).
[12] T. Senthil, J. B. Marston, and M. P. A. Fisher, Spin quantum Hall effect in unconventional superconductors, Phys. Rev. B **60**, 4245 (1999).
[13] N. Read and D. Green, Paired states of fermions in two dimensions with breaking of parity and time-reversal symmetries and the fractional quantum Hall effect, Phys. Rev. B **61**, 10267 (2000).
[14] M. Titov, P. W. Brouwer, A. Furusaki, and C. Mudry, Fokker-Planck equations and density of states in disordered quantum wires, Phys. Rev. B **63**, 235318 (2001).
[15] B. L. Altshuler, Y. Gefen, A. Kamenev, and L. S. Levitov, Quasiparticle Lifetime in a Finite System: A Nonperturbative Approach, Phys. Rev. Lett. **78**, 2803 (1997).
[16] I. V. Gornyi, A. D. Mirlin, and D. G. Polyakov, Interacting Electrons in Disordered Wires: Anderson Localization and Low-T Transport, Phys. Rev. Lett. **95**, 206603 (2005).
[17] D. M. Basko, I. L. Aleiner, and B. L. Altshuler, Metal insulator transition in a weakly interacting many electron system with localized single particle states, Ann. Phys. **321**, 1126 (2006).
[18] D. A. Abanin and Z. Papić, Recent progress in many-body localization, Ann. Phys. (Berlin) **529**, 1700169 (2017).
[19] F. Alet and N. Laflorencie, Many-body localization: An introduction and selected topics, C. R. Phys. **19**, 498 (2018).

[20] M. Filoche and S. Mayboroda, Universal mechanism for anderson and weak localization, Proc. Natl. Acad. Sci. USA **109**, 14761 (2012).

[21] M. Filoche and S. Mayboroda, The landscape of Anderson localization in a disordered medium, in *Fractal Geometry and Dynamical Systems in Pure and Applied Mathematics II: Fractals in Applied Mathematics*, edited by D. Carfi *et al.*, Contemporary Mathematics Vol. 601 (American Mathematical Society, Providence, RI, 2013), p. 103.

[22] M. L. Lyra, S. Mayboroda, and M. Filoche, Dual hidden landscapes in Anderson localization on discrete lattices, Europhys. Lett. **109**, 47001 (2014).

[23] D. N. Arnold, G. David, D. Jerison, S. Mayboroda, and M. Filoche, Effective Confining Potential of Quantum States in Disordered Media, Phys. Rev. Lett. **116**, 056602 (2016).

[24] S. Steinerberger, Localization of Quantum States and Landscape Functions, Proc. Am. Math. Soc. **145**, 2895 (2017).

[25] M. Filoche, M. Piccardo, Y.-R. Wu, C.-K. Li, C. Weisbuch, and S. Mayboroda, Localization landscape theory of disorder in semiconductors. I. Theory and modeling, Phys. Rev. B **95**, 144204 (2017).

[26] M. Piccardo, C.-K. Li, Y.-R. Wu, J. S. Speck, B. Bonef, R. M. Farrell, M. Filoche, L. Martinelli, J. Peretti, and C. Weisbuch, Localization landscape theory of disorder in semiconductors. II. Urbach tails of disordered quantum well layers, Phys. Rev. B **95**, 144205 (2017).

[27] C.-K. Li, M. Piccardo, L.-S. Lu, S. Mayboroda, L. Martinelli, J. Peretti, J. S. Speck, C. Weisbuch, M. Filoche, and Y.-R. Wu, Localization landscape theory of disorder in semiconductors. III. Application to carrier transport and recombination in light emitting diodes, Phys. Rev. B **95**, 144206 (2017).

[28] D. N. Arnold, G. David, M. Filoche, D. Jerison, and S. Mayboroda, Computing spectra without solving eigenvalue problems, SIAM J. Sci. Comput. **41**, B69 (2019).

[29] G. David, M. Filoche, and S. Mayboroda, The landscape law for the integrated density of states, arXiv:1909.10558.

[30] G. Lemut, M. J. Pacholski, O. Ovdat, A. Grabsch, J. Tworzydło, and C. W. J. Beenakker, Localization landscape for Dirac fermions, Phys. Rev. B **101**, 081405(R) (2020).

[31] A. Ostrowski, Über die determinanten mit überwiegender hauptdiagonale, Comment. Math. Helv. **10**, 69 (1937).

[32] A. Ostrowski, Determinanten mit überwiegender hauptdiagonale und die absolute konvergenz von linearen iterationsprozessen, Comment. Math. Helv. **30**, 175 (1956).

[33] L. Collatz, *Functional Analysis and Numerical Mathematics* (Academic, New York, 1966).

[34] B. L. Buzbee, G. H. Golub, and C. W. Nielson, On direct methods for solving Poisson's equations, SIAM J. Numer. Anal. **7**, 627 (1970).

[35] A. George, Nested dissection of a regular finite element mesh, SIAM J. Numer. Anal. **10**, 345 (1973).

[36] M. P. L. Sancho, J. M. L. Sancho, J. M. L. Sancho, and J. Rubio, Highly convergent schemes for the calculation of bulk and surface Green functions, J. Phys. F **15**, 851 (1985).

[37] A. Svizhenko, M. P. Anantram, T. R. Govindan, B. Biegel, and R. Venugopal, Two-dimensional quantum mechanical modeling of nanotransistors, J. Appl. Phys. **91**, 2343 (2002).

[38] C. H. Lewenkopf and Eduardo R. Mucciolo, The recursive Green's function method for graphene, J. Comput. Electron. **12**, 203 (2013).

[39] S. Li, S. Ahmed, G. Klimeck, and E. Darve, Computing entries of the inverse of a sparse matrix using the find algorithm, J. Comput. Phys. **227**, 9408 (2008).

[40] L. Lin, J. Lu, L. Ying, R. Car, and E. Weinan, Fast algorithm for extracting the diagonal of the inverse matrix with application to the electronic structure analysis of metallic systems, Commun. Math. Sci. **7**, 755 (2009).

[41] S. Li and E. Darve, Extension and optimization of the find algorithm: Computing Green's and less-than Green's functions, J. Comput. Phys. **231**, 1121 (2012).

[42] P. D. Robinson and A. J. Wathen, Variational bounds on the entries of the inverse of a matrix, IMA J. Numer. Anal. **12**, 463 (1992).

[43] G. Golub and G. Meurant, Matrices, moments and quadrature, in *Numerical Analysis 1993*, Pitman Research Notes in Mathematics Series Vol. 303 (Longman Scientific, Essex, U.K., 1994), p. 105.

[44] M. Benzi and G. H. Golub, Bounds for the entries of matrix functions with applications to preconditioning, BIT Numer. Math. **39**, 417 (1999).

[45] T. Morimoto, A. Furusaki, and C. Mudry, Anderson localization and the topology of classifying spaces, Phys. Rev. B **91**, 235111 (2015).

[46] J. H. Bardarson, J. Tworzydło, P. W. Brouwer, and C. W. J. Beenakker, One-Parameter Scaling at the Dirac Point in Graphene, Phys. Rev. Lett. **99**, 106801 (2007).

[47] K. Nomura, M. Koshino, and S. Ryu, Topological Delocalization of Two-Dimensional Massless Dirac Fermions, Phys. Rev. Lett. **99**, 146806 (2007).

[48] P. M. Ostrovsky, I. V. Gornyi, and A. D. Mirlin, Quantum Criticality and Minimal Conductivity in Graphene with Long-Range Disorder, Phys. Rev. Lett. **98**, 256801 (2007).

[49] T. Senthil and M. P. A. Fisher, Quasiparticle localization in superconductors with spin-orbit scattering, Phys. Rev. B **61**, 9690 (2000).

[50] J. H. Bardarson, M. V. Medvedyeva, J. Tworzydło, A. R. Akhmerov, and C. W. J. Beenakker, Absence of a metallic phase in charge-neutral graphene with a random gap, Phys. Rev. B **81**, 121414(R) (2010).

[51] M. V. Medvedyeva, J. Tworzydło, and C. W. J. Beenakker, Effective mass and tricritical point for lattice fermions localized by a random mass, Phys. Rev. B **81**, 214203 (2010).

[52] M. Wimmer, A. R. Akhmerov, M. V. Medvedyeva, J. Tworzydło, and C. W. J. Beenakker, Majorana Bound States without Vortices in Topological Superconductors with Electrostatic Defects, Phys. Rev. Lett. **105**, 046803 (2010).

[53] A. W. W. Ludwig, M. P. A. Fisher, R. Shankar, and G. Grinstein, Integer quantum Hall transition: An alternative approach and exact results, Phys. Rev. B **50**, 7526 (1994).

[54] A. Altland, Spectral and transport properties of d-wave superconductors with strong impurities, Phys. Rev. B **65**, 104525 (2002).

[55] P. M. Ostrovsky, I. V. Gornyi, and A. D. Mirlin, Conductivity of disordered graphene at half filling, Eur. Phys. J.: Spec. Top. **148**, 63 (2007).

[56] See Supplemental Material at http://link.aps.org/supplemental/10.1103/PhysRevB.101.220201 for more details.

[57] S. Balasubramanian, Y. Liao, and V. Galitski, Many-body localization landscape, Phys. Rev. B **101**, 014201 (2020).

[58] M. Janssen, Multifractal analysis of broadly-distributed observables at criticality, Int. J. Mod. Phys. B **08**, 943 (1994).

[59] B. Huckestein, Scaling theory of the integer quantum Hall effect, Rev. Mod. Phys. **67**, 357 (1995).

[60] C. Mudry, C. Chamon, and X.-G. Wen, Two-dimensional conformal field theory for disordered systems at criticality, Nucl. Phys. B **466**, 383 (1996).

[61] C. C. Chamon, C. Mudry, and X.-G. Wen, Localization in Two Dimensions, Gaussian Field Theories, and Multifractality, Phys. Rev. Lett. **77**, 4194 (1996).

[62] F. Evers and A. D. Mirlin, Fluctuations of the Inverse Participation Ratio at the Anderson Transition, Phys. Rev. Lett. **84**, 3690 (2000).

[63] F. Evers, A. Mildenberger, and A. D. Mirlin, Multifractality of wave functions at the quantum Hall transition revisited, Phys. Rev. B **64**, 241303(R) (2001).

[64] T. Nakayama and K. Yakubo, Multifractals in the Anderson transition, in *Fractal Concepts in Condensed Matter Physics* (Springer, Berlin, 2003), pp. 149–176.